Design of a High Performance Mid-IR Fiber Laser Based on Pr^{3+}-Doped Fluoroindate Glass

Antonella Maria Loconsole, Vito Vincenzo Francione, Andrea Annunziato, Francesco Anelli, *Student Member, IEEE*, and Francesco Prudenzano, *Member, IEEE*

***Abstract*—In this work, a novel continuous wave fiber laser, pumped at $\lambda_p = 1550$ nm and emitting at $\lambda_s = 4$ μm, has been designed and optimized. It is based on a step-index, double-cladding, praseodymium-doped fluoroindate glass fiber, available on market, having dopant concentration $N_{Pr} = 8000$ ppm. For a realistic design, measured spectroscopical parameters have been taken into account, writing a five-level rate equation model. The design is carried out by employing a homemade code solver. The best predicted slope efficiency of about $\eta = 33\%$ and pump power threshold $P_{th} = 0.007$ W have been obtained for a fiber length $L_{fiber} = 0.4$ m and output mirror reflectivity $R_{out} = 30\%$. These values are very interesting with reference to the state of the art and promise the fabrication of high beam quality optical sources in the middle infrared range, by employing conventional erbium-doped fiber pumping lasers, with a potentially easy all-in-fiber integration.**

***Index Terms*—Electromagnetic design, fiber laser, fluoroindate, middle infrared, praseodymium.**

I. Introduction

During the recent years, middle-infrared (Mid-IR) sources have been intensely investigated, paving the way of faster communications, novel imaging, medical and environmental applications, thanks to the absorption peaks shown by many compounds in this wavelength range [1], [2]. They can be integrated in all-in-fiber systems, by employing couplers, combiners, and Fiber Bragg Gratings (FBG), to obtain compact and low-loss architectures [3], [4]. Fiber lasers and amplifiers can be fabricated with several glasses, depending on their operation wavelength range, including silicate, tellurite, chalcogenide, and fluoride, doped or co-doped with different rare-earth ions, such as erbium, ytterbium, holmium, praseodymium, neodymium, or europium [5], [6], [7], [8], [9], [10], [11], [12], [13], [14], [15], [16]. Fluoroindate glasses are promising hosts thanks to their low phonon energy (≈ 510 cm^{-1}), high transparency from UV till 5 μm wavelength ($\alpha < 1$ dB/m), and high rare-earth ions solubility [6]. Typical background losses, measured via cut-back method are $\alpha < 10$ dB/km at 3670 nm [17]. Recently, the design of continuous wave (CW) and pulsed lasers operating in the Mid-IR range have shown promising results. Erbium-doped fluoroindate fiber lasers have been widely investigated to operate around $\lambda_s = 3.4$ μm, by employing a dual-wavelength pumping at $\lambda_p = 974$ nm and $\lambda_p = 1976$ nm, showing slope efficiency of $\eta = 19\%$ [7], [8]. Also emission till $\lambda_s = 3.91$ μm has been predicted with erbium-doped fluoroindate fiber lasers, considering pumping at $\lambda_p = 635$ nm, with a maximum slope efficiency $\eta = 1.6\%$ and pump power threshold $P_{th} = 25$ mW [9]. Holmium-heavily-doped fluoroindate fibers have been employed to design CW and gain-switching pulsed lasers emitting at $\lambda_s = 3.92$ μm, when pumped at $\lambda_p = 888$ nm, with a slope efficiency around $\eta = 10\%$ for the CW laser [10], [11]. The low value of the slope efficiency is due to holmium transition $I_5 \rightarrow I_6$, which is self-terminating. This inconvenience can be reduced by considering a second pumping at $\lambda_p = 976$ nm or $\lambda_p = 1660$ nm, or co-doping with neodymium or europium ions [12], [13], [14], [15]. The simulation of dual-wavelength pumping promises a slightly higher slope efficiency of $\eta = 12.1\%$ [13] while co-doping holmium with neodymium has been proposed to obtain a slope efficiency $\eta = 16.67\%$, and pump power threshold $P_{th} = 0.2$ W. Lastly, dysprosium-doped fluoroindate fiber lasers have been designed for emitting at $\lambda_s = 4.4$ μm, when pumped at $\lambda_p = 1.7$ μm [18], [19], showing slope efficiency $\eta \approx 27\%$ and high pump power threshold $P_{th} \approx 30$ W, for the CW laser with cascade emission at $\lambda_s = 3.3$ μm and $\lambda_s = 4.4$ μm. Recent spectroscopical studies include the activation of fluoroindate fibers with ions of dysprosium and terbium [20], praseodymium, and praseodymium and ytterbium [21]. They have exhibited emission at $\lambda_s = 4$ μm by pumping at $\lambda_p = 1550$ nm, in the case of praseodymium-doped fluoroindate fibers, and by pumping at $\lambda_p = 980$ nm, in the case of praseodymium/ytterbium co-doped fluoroindate fibers [21].

In this work, for the first time to the best of our knowledge, a continuous wave laser based on a Pr^{3+}-doped fluoroindate fiber, emitting at $\lambda_s = 4$ μm when pumped at $\lambda_p = 1550$ nm,

Manuscript received 29 September 2023; revised 15 November 2023; accepted 24 November 2023. Date of publication 1 December 2023; date of current version 2 April 2024. This work was supported in part by the research projects: H2020-ICT-37-2020 Photonic Accurate and Portable Sensor Systems Exploiting Photo-Acoustic and Photo-Thermal Based Spectroscopy for Real-Time Outdoor Air Pollution Monitoring—PASSEPARTOUT under Grant 10101695\6, in part by European Union through the Italian National Recovery and Resilience Plan (NRRP) of NextGenerationEU, "Telecommunications of the Future" (PE00000001—program "RESTART," CUP: D93C22000910001) - project DREAMS—"Antennas & Devices foR mixing, dEtection And Manipulation of mmWaves", in part by MIUR "Agriculture Green & Digital—AGREED," PNR 2015/20, under Grant ARS01_00254, and in part by MIUR PRIN 2022, PNRR "InnoVative tEchnoloGies for non-invasivE assessmenT of plAnt healTh conditIon to support precisiOn farmiNg—VEGETATION"—DD under Grant 1181 del 27-07-2023. *(Corresponding author: Francesco Prudenzano.)*

The authors are with the Department of Electrical and Information Engineering, Politecnico di Bari, 70125 Bari, Italy (e-mail: antonellamaria.loconsole@poliba.it; v.francione@phd.poliba.it; andrea.annunziato@poliba.it; francesco.anelli@poliba.it; francesco.prudenzano@poliba.it).

Color versions of one or more figures in this article are available at https://doi.org/10.1109/JLT.2023.3338139.

Digital Object Identifier 10.1109/JLT.2023.3338139

© 2023 The Authors. This work is licensed under a Creative Commons Attribution 4.0 License. For more information, see https://creativecommons.org/licenses/by/4.0/

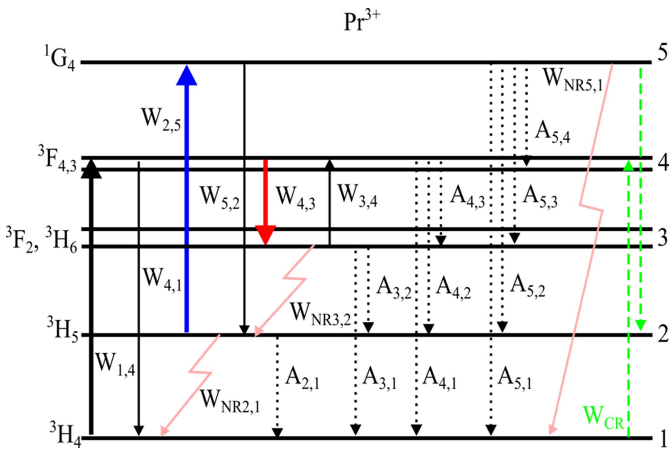

Fig. 1. Energy levels scheme, including pumping (bold black arrow), stimulated emission (bold red arrow), radiative (dotted arrows) and non-radiative (lightning arrows) emissions, excited state absorption (ESA) (blue bold arrow), and cross-relaxation (CR) (green dashed arrows) phenomena.

has been designed and optimized, starting from experimental spectroscopical parameters taken from literature [21], [22], [23], [24], [25], [26] and employing a home-made computer code solver [14].

II. Recall of Theory

The praseodymium-doped glass emitting at $\lambda_s = 4\ \mu$m when pumped at $\lambda_p = 1550$ nm is modeled with a 5-level scheme, as reported in Fig. 1. It takes into account pumping (bold black arrow), stimulated emission (bold red arrow), radiative and non-radiative emissions, Excited State Absorption (ESA), and cross-relaxation (CR) phenomena.

By considering a rate equation approach, the following non-linear system (1a)–(1e) can be written to evaluate the ion populations $N_1, \ldots, N_5$.

$$\frac{\partial N_1}{\partial t} = -W_{14}N_1 + W_{41}N_4 + A_{51}N_5 + A_{41}N_4 + A_{31}N_3 + A_{21}N_2 + W_{NR21}N_2 - W_{CR}N_1N_5 + W_{NR51}N_5 \quad (1a)$$

$$\frac{\partial N_2}{\partial t} = -W_{25}N_2 + W_{52}N_5 - \frac{1}{\tau_{R2}}N_2 + A_{52}N_5 + A_{42}N_4 + A_{32}N_3 + W_{CR}N_1N_5 + W_{NR32}N_3 - W_{NR21}N_2 \quad (1b)$$

$$\frac{\partial N_3}{\partial t} = -W_{34}N_3 + W_{43}N_4 - \frac{1}{\tau_{R3}}N_3 + A_{53}N_5 + A_{43}N_4 - W_{NR32}N_3 \quad (1c)$$

$$\frac{\partial N_4}{\partial t} = W_{14}\,N_1 - W_{41}N_4 - W_{43}N_4 + W_{34}N_3 - \frac{1}{\tau_{R4}}N_4 + A_{54}N_5 + W_{CR}N_1N_5 \quad (1d)$$

$$\frac{\partial N_5}{\partial t} = W_{25}\,N_2 - W_{52}N_5 - \frac{1}{\tau_{R5}}N_5 - W_{CR}N_1N_5 - W_{NR51}N_5 \quad (1e)$$

where $A_{i,j} = \frac{\beta_{i,j}}{\tau_i}$ are the radiative decays, $\beta_{i,j}$ are the branching ratios, τ_i are the i-th level lifetimes, W_{CR} is the cross relaxation rate, and $W_{NR,ij}$ are the non-radiative decay rates. The ion population condition $N_{Pr} = N_1 + N_2 + N_3 + N_4 + N_5$ is considered. The coefficients W_{ij} are the transition rates for $i \rightarrow j$ transition defined as

$$W_{i,j} = \frac{\sigma_{i,j}\left(\lambda_{p/s}\right)}{h\nu_{p/s}A_d}\,P_{p/s}\Gamma_{p/s} \quad (2)$$

where $\sigma_{i,j}(\lambda_{p/s})$ is the emission/absorption cross section at the wavelength $\lambda_{p/s}$ for the $i \rightarrow j$ transition, h is the Planck constant, $\nu_{p/s}$ is the pump/signal frequency, P_p is the pump power, P_s is the forward signal power, Γ_p and Γ_s are the overlap coefficients of pump and signal beams with the doped area A_d, respectively.

The power propagation along the fiber, for the pump P_p and for the signal P_s, is modeled by considering the following equations:

$$\frac{\partial P_p}{\partial z} = \left[g_p\left(z\right) - \alpha\right]\ P_p\left(z\right) \quad (3a)$$

$$\frac{\partial P_s^{\pm}}{\partial z} = \pm\left[g_s\left(z\right) - \alpha\right] P_s^{\pm}\left(z\right) \quad (3b)$$

where α is the glass attenuation, and g_p and g_s are the pump and signal gains, respectively, defined as:

$$g_p\left(z\right) = \left[-\sigma_{14}\left(\nu_p\right)N_1\left(z\right) + \sigma_{41}\left(\nu_p\right)N_4\left(z\right)\right]\ \Gamma_p + \left[-\sigma_{25}\left(\nu_p\right)N_2\left(z\right) + \sigma_{52}\left(\nu_p\right)N_5\left(z\right)\right]\Gamma_p,$$

$$g_s\left(z\right) = \left[-\sigma_{34}\left(\nu_s\right)N_3\left(z\right) + \sigma_{43}\left(\nu_s\right)N_4\left(z\right)\right]\ \Gamma_s.$$

The following boundaries conditions are imposed:

$$P_p\left(0\right) = P_p \quad (4a)$$

$$P_s^{+}\left(0\right) = R_{in}\ P_s^{-}\left(0\right) \quad (4b)$$

$$P_s^{-}\left(L\right) = R_{out}\ P_s^{+}\left(L\right) \quad (4c)$$

where $z = 0$ and $z = L$ represent the ends of the laser cavity, P_p is the input pump power, R_{in} and R_{out} are the input and output mirror reflectivity, respectively. Initial conditions for level populations are also imposed as follows:

$$N_1\ (0) = N_{Pr} \quad (4d)$$

$$N_2\ (0) = N_3\ \ (0) = N_4\ \ (0) = N_5\ \ (0) = 0 \quad (4e)$$

III. Laser Design

The laser has been designed considering a step-index double-cladding fluoroindate fiber doped with praseodymium concentration $N_{Pr} = 1.6 \times 10^{26}$ ions/m^3 = 8000 ppm, by Le Verre Fluoré [17]. Fig. 2 shows the fiber cross-section geometry and the HE_{11} mode at the signal wavelength. It has core diameter $d_{co} = 7.5\ \mu$m, inner cladding of diameter $d_{cl1} = 125\ \mu$m shaped with a 2-D cut at distance $d = 115\ \mu$m, and second cladding diameter $d_{cl2} = 180\ \mu$m. The parameters employed for modeling are reported in Table I. The fiber has been investigated via a

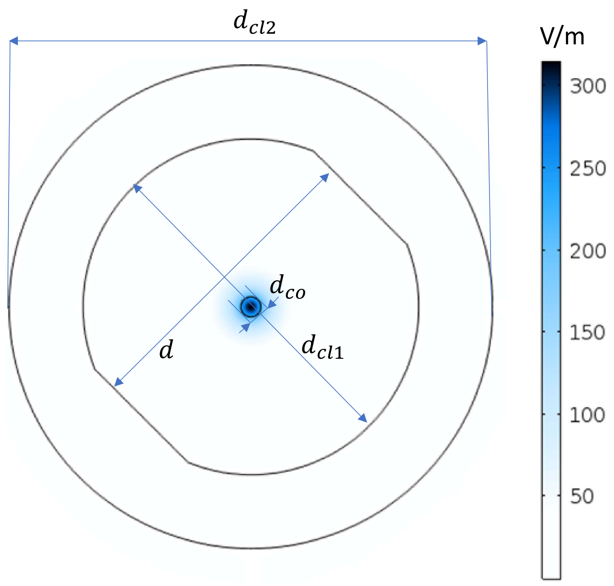

Fig. 2. Fiber cross-section geometry and E-field modulus of the fundamental mode HE_{11} at signal wavelength λ_s.

TABLE I
MODELING PARAMETERS

Symbol	Value	Description
λ_p	1550 nm	Pump wavelength
λ_s	4000 nm	Signal wavelength
d_{co}	7.5 μm	Core diameter
d	115 μm	2-D cut distance
d_{cl1}	125 μm	Inner cladding diameter
d_{cl2}	180 μm	Outer cladding diameter
N_{Pr}	8000 ppm	Dopant concentration
R_{in}	95 %	Input mirror reflectivity
R_{out}	30 ÷ 80 %	Output mirror reflectivity
L_{fiber}	0.3 ÷ 0.7 m	Fiber length
$\alpha(\lambda_p)$	0.1 dB/m [17]	Glass attenuation at pump wavelength
$\alpha(\lambda_s)$	0.01 dB/m [17]	Glass attenuation at signal wavelength
$n_{co}(\lambda_p)$	1.4881	Core refractive index at pump wavelength
$n_{co}(\lambda_s)$	1.4721	Core refractive index at signal wavelength
$n_{cl1}(\lambda_p)$	1.4746	Inner cladding refractive index at pump wavelength
$n_{cl1}(\lambda_s)$	1.4585	Inner cladding refractive index at signal wavelength
$n_{cl2}(\lambda_p)$	1.3872	Outer cladding refractive index at pump wavelength
$n_{cl2}(\lambda_s)$	1.3785	Outer cladding refractive index at signal wavelength

Finite Element Method (FEM) software, in order to calculate the pump and the signal overlap coefficients $\Gamma_p = 0.899$ and $\Gamma_s = 0.312$, respectively. The fiber is monomodal at signal wavelength. Table II reports the experimental spectroscopical parameters employed in the design, taken from literature.

The design is carried out via a home-made solver code, the structure of which is based on the rate-equations approach, well validated in a number of cases [9], [11], [14]. In the design, several simulations have been carried out to investigate the behavior

TABLE II
SPECTROSCOPIC PARAMETERS OF PR^{3+}-DOPED FLUOROINDATE GLASS FIBER

Symbol	Value	Description
$\sigma_{14}(\lambda_p)$	$1.2 \times 10^{-24}\ m^2$ [22]	Absorption cross section $H_4 \rightarrow H_5$
$\sigma_{41}(\lambda_p)$	$1.2 \times 10^{-24}\ m^2$ [22]	Emission cross section $H_5 \rightarrow H_4$
$\sigma_{25}(\lambda_p)$	$2.0 \times 10^{-25}\ m^2$ [26]	Absorption cross section $H_5 \rightarrow G_4$
$\sigma_{52}(\lambda_p)$	$4.8 \times 10^{-25}\ m^2$ [26]	Emission cross section $G_4 \rightarrow H_5$
$\sigma_{34}(\lambda_s)$	$6.5 \times 10^{-25}\ m^2$ [21]	Absorption cross section $F_2, H_6 \rightarrow F_{4,3}$
$\sigma_{43}(\lambda_s)$	$1.44 \times 10^{-24}\ m^2$ [21]	Emission cross section $F_{4,3} \rightarrow F_2, H_6$
τ_5	2.35 ms [21]	G_4 radiative lifetime
τ_4	2.28 ms [21]	$F_{4,3}$ radiative lifetime
τ_3	57 ms [23]	H_6 radiative lifetime
τ_2	79 ms [23]	H_5 radiative lifetime
β_{21}	100%	$H_5 \rightarrow H_4$ branching ratio
β_{31}	62.23% [25]	$H_6 \rightarrow H_4$ branching ratio
β_{32}	37.77% [25]	$H_6 \rightarrow H_5$ branching ratio
β_{41}	63.06% [21]	$F_{4,3} \rightarrow H_4$ branching ratio
β_{42}	27.71% [21]	$F_{4,3} \rightarrow H_5$ branching ratio
β_{43}	9.24% [21]	$F_{4,3} \rightarrow F_2, H_6$ branching ratio
β_{51}	5.81% [21]	$G_4 \rightarrow H_4$ branching ratio
β_{52}	61.26% [21]	$G_4 \rightarrow H_5$ branching ratio
β_{53}	28.34% [21]	$G_4 \rightarrow F_2, H_6$ branching ratio
β_{54}	4.57% [21]	$G_4 \rightarrow F_{4,3}$ branching ratio
W_{NR51}	14514 s^{-1} [24]	Non-radiative rate $G_4 \rightarrow H_4$
W_{NR32}	6664 s^{-1} [25]	Non-radiative rate $H_6 \rightarrow H_5$
W_{NR21}	499987 s^{-1} [23]	Non-radiative rate $H_5 \rightarrow H_4$
W_{CR}	$2.25 \times 10^4\ s^{-1}$ [23]	Cross relaxation rate

of the laser output power P_s as a function of the input pump power, for different values of: (i) the fiber length L_{fiber}, and (ii) the output mirror reflectivity R_{out}. Moreover, also the behavior of the laser output power P_s as a function of (iii) the fiber length L_{fiber}, and (iv) the output mirror reflectivity R_{out}, for different values of the input pump power has been investigated. The input mirror reflectivity is kept fixed to $R_{in} = 95\%$, as a cautionary value to simulate a Fiber Bragg Grating (FBG) in an all-in-fiber set-up.

Fig. 3(a) shows the laser output power P_s as a function of the input pump power, for different values of the fiber length L_{fiber}, i.e., laser cavity. The slope efficiency tends to slightly reduce for longer fibers, whereas the saturation pump power P_{sat} increases. Fig. 3(b) shows an enlarged view to better observe the threshold P_{th}. The pump power threshold P_{th} slightly increases as the fiber length L_{fiber} increases. The best value is obtained for $L_{fiber} = 0.4$ m, $P_{th} = 0.003$ W, while the saturation pump power is $P_{sat} = 1.3$ W, corresponding to the laser output power $P_s = 0.34$ W. The slope efficiency is $\eta = 28\%$.

Fig. 4(a) shows the laser output power P_s as a function of the input pump power, for different values of the output mirror reflectivity R_{out}. As the reflectivity decreases, the slope efficiency asymptotically increases reaching $\eta = 32.5\%$, for $R_{out} = 30\%$, while the saturation pump power P_{sat} remains almost the same in all cases. The maximum laser output power is $P_s = 0.42$ W. The pump power threshold P_{th} slightly increases as the output mirror reflectivity decreases, but it is always below $P_{th} < 10$ mW, as better illustrated in Fig. 4(b).

Fig. 5 shows the laser output power P_s as a function of the output mirror reflectivity R_{out}, for different values of the input

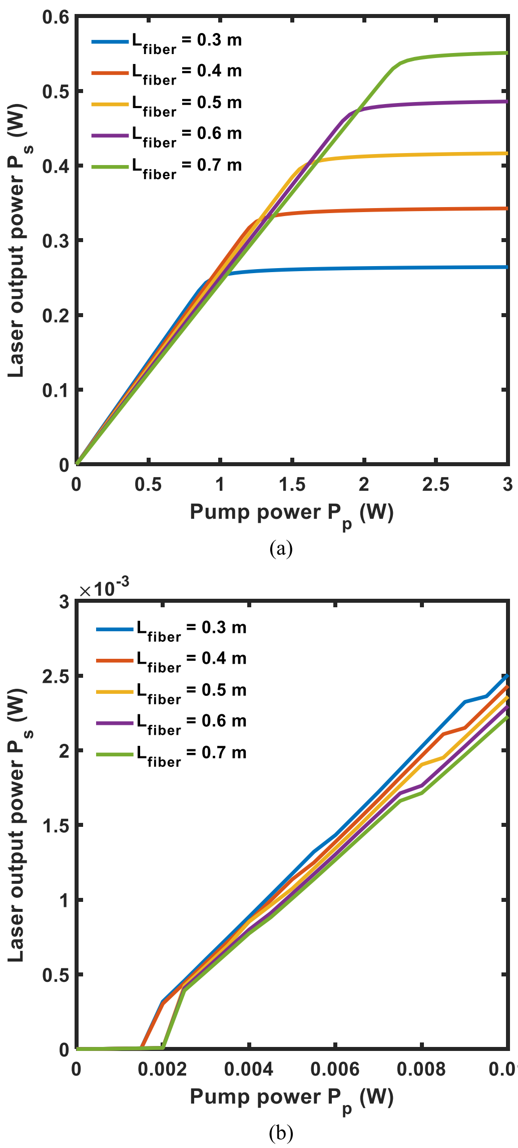

Fig. 3. Laser output power P_s as a function of the input pump power P_p, for different values of the fiber length L_{fiber}, input mirror reflectivity $R_{in} = 95\%$, output mirror reflectivity $R_{out} = 80\%$; (b) enlarged view of the pump power threshold.

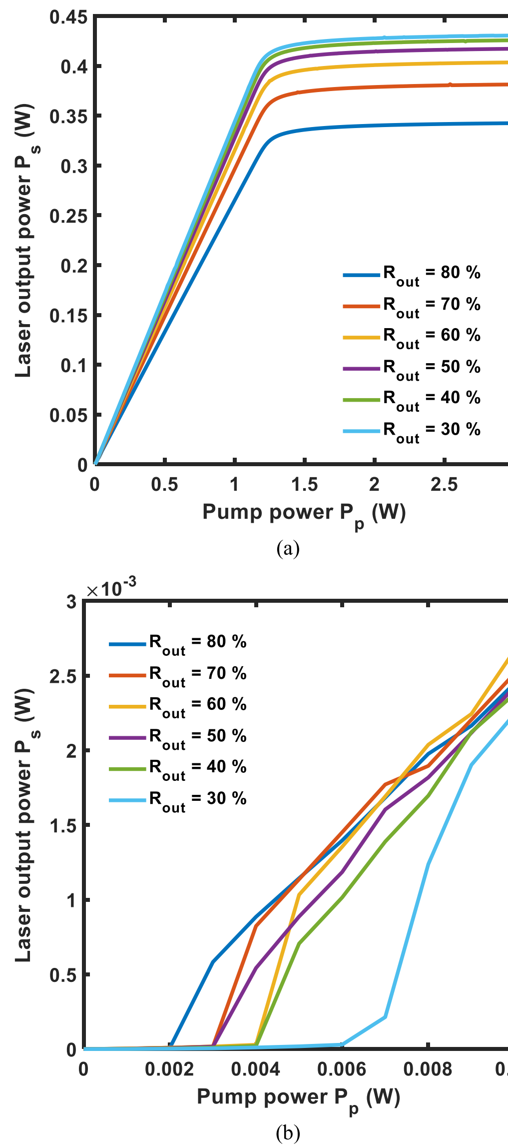

Fig. 4. Laser output power P_s as a function of the input pump power P_p, for different values of the output mirror reflectivity R_{out}, input mirror reflectivity $R_{in} = 95\%$, fiber length $L_{fiber} = 0.4$ m; (b) enlarged view of the pump power threshold.

pump power P_p. The laser output power P_s slowly increases for lower values of the output mirror reflectivity R_{out}, as also shown in Fig. 4. As the input pump power P_p increases, the variation of the output power becomes more evident.

Fig. 6 shows the laser output power P_s as a function of the fiber length L_{fiber}, for different values of the input pump power P_p. For each value of the input pump power, a saturation of the laser output power can be observed.

Table III reports a comparison among the Pr^{3+}-doped fluoroindate fiber laser proposed in this work and other fluoroindate fiber lasers emitting in Mid-IR [8], [9], [10], [12], [13], [14], [18]. In particular, the comparison with literature is performed in terms of doping ion, emission wavelength λ_s, pump wavelength λ_p, pump power threshold P_{th}, and slope efficiency η. All the considered lasers emit between $\lambda_s = 3.4$ μm and $\lambda_s = 4.4$ μm, and are pumped in the visible or near-infrared (NIR) range. It is worth noting that in [8], [12], [13], dual-wavelength pumping schemes are proposed to increase the slope efficiency and to reduce the pump power threshold. The proposed laser exhibits the highest slope efficiency and the lowest pump power threshold, with one of the longest emitting wavelengths. Moreover, it can be pumped by employing a commercial erbium-doped fiber laser, to be spliced with the praseodymium-doped fiber, available on the market, thus obtaining an all-in-fiber device, with FGBs employed as cavity mirrors [4]. The possibility to employ a single pumping wavelength simplifies the construction scheme of the laser system. Fluoride erbium-doped fiber lasers could be taken into account [7], [8], [9] with a proper design to emit at 1.5 μm.

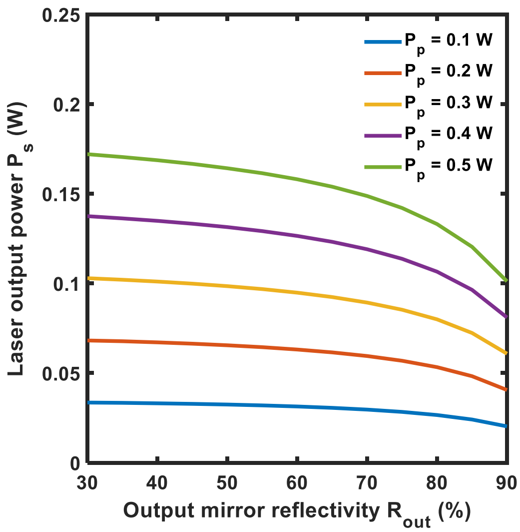

Fig. 5. Laser output power P_s as a function of the output mirror reflectivity R_{out}, for different values of the input pump power P_p, input mirror reflectivity $R_{in} = 95\%$, fiber length $L_{fiber} = 0.4$ m.

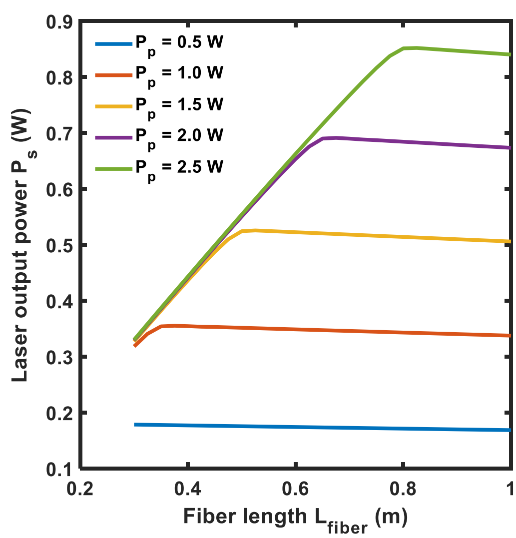

Fig. 6. Laser output power P_s as a function of the fiber length L_{fiber}, for different values of the input pump power P_p, input mirror reflectivity $R_{in} = 95\%$, output mirror reflectivity $R_{out} = 30\%$.

IV. Conclusion

For the first time to the best of our knowledge, a fiber laser based on a praseodymium-doped fluoroindate glass, emitting at $\lambda_s = 4\ \mu$m, when pumped at $\lambda_p = 1550$ nm, has been designed and optimized, by considering spectroscopical parameters taken from literature. The predicted slope efficiency $\eta = 33\%$ is promising, along with the low input pump threshold. NIR pumping could be implemented by employing an erbium-doped fiber laser, spliced with the praseodymium fluoroindate fiber cavity. Future developments may consider co-doping with ytterbium, to obtain multi-wavelength emission at both $\lambda_s = 3.6\ \mu$m and $\lambda_s = 4\ \mu$m.

TABLE III
Comparison of Laser Performance With Other Mid-IR Lasers Based on Fluoroindate Fibers

Ref.	Dopant	Emitting wavelength λ_s	Pump wavelength λ_p	Pump power threshold P_{th}	Slope efficiency η
[8]	Er^{3+}	3.44 µm	972 nm 1976 nm	-	19 %
[9]	Er^{3+}	3.91 µm	635 nm	25 mW	1.6 %
[10]	Ho^{3+}	3.92 µm	888 nm	4.3 W	10.2 %
[12]	Ho^{3+}	3.92 µm	888 nm 962 nm	-	19 %
[13]	Ho^{3+}	3.92 µm	888 nm 1660 nm	2 W	12.1 %
[14]	Ho^{3+}/ Nd^{3+}	3.92 µm	808 nm	200 mW	16.7 %
[18]	Dy^{3+}	3.3 µm 4.4 µm	1700 nm	30 W	27 %
This work	Pr^{3+}	4 µm	1550 nm	7 mW	33 %

References

[1] X. Li, X. Huang, X. Hu, X. Guo, and Y. Han, "Recent progress on mid-infrared pulsed fiber lasers and the applications," *Opt. Laser Technol.*, vol. 158, 2023, Art. no. 108898.

[2] A. E. Klingbeil, J. B. Jeffries, and R. K. Hanson, "Temperature-dependent mid-IR absorption spectra of gaseous hydrocarbons," *J. Quantitative Spectrosc. Radiat. Transfer*, vol. 107, no. 3, pp. 407–420, Oct. 2007.

[3] A. Annunziato, F. Anelli, P. Le Pays Du Teilleul, S. Cozic, S. Poulain, and F. Prudenzano, "Fused optical fiber combiner based on indium fluoride glass: Perspectives for mid-IR applications," *Opt. Exp.*, vol. 30, pp. 44160–44174, 2022.

[4] G. Bharathan et al., "Femtosecond laser direct-written fiber Bragg gratings with high reflectivity and low loss at wavelengths beyond 4μm," *Opt. Lett.*, vol. 45, no. 15, 2020, Art. no. 4316.

[5] L. Sójka et al., "High peak power q-switched Er:ZBLAN fiber laser," *J. Lightw. Technol.*, vol. 39, no. 20, pp. 6572–6578, Oct. 2021.

[6] L. Zhang, F. Guan, L. Zhang, and Y. Jiang, "Next generation mid-infrared fiber: Fluoroindate glass fiber," *Opt. Mater. Exp.*, vol. 12, pp. 1683–1707, 2022.

[7] O. Henderson-Sapir, A. Malouf, N. Bawden, J. Munch, S. D. Jackson, and D. J. Ottaway, "Recent advances in 3.5 μm erbium-doped mid-infrared fiber lasers," *IEEE J. Sel. Topics Quantum Electron.*, vol. 23, no. 3, May/Jun. 2017, Art. no. 0900509.

[8] V. Fortin, F. Maes, M. Bernier, S. T. Bah, M. D'Auteuil, and R. Vallée, "Watt-level erbium-doped all-fiber laser at 3.44 μm," *Opt. Lett.*, vol. 41, pp. 559–562, 2016.

[9] M. C. Falconi, A. M. Loconsole, A. Annunziato, S. Cozic, S. Poulain, and F. Prudenzano, "Design of a broadband erbium-doped fluoroindate fiber laser emitting up to 3.91 μm," *J. Lightw. Technol.*, vol. 41, no. 18, pp. 6065–6072, Sep. 2023.

[10] F. Maes et al., "Room-temperature fiber laser at 3.92 μm," *Optica*, vol. 5, no. 7, pp. 761–764, Jul. 2018.

[11] A. M. Loconsole, M. C. Falconi, V. Portosi, and F. Prudenzano, "Numerical design of a gain-switched pulsed laser at 3.92 μm wavelength based on a Ho3+-doped fluoroindate fiber," *J. Lightw. Technol.*, vol. 39, no. 10, pp. 3276–3283, May 2021.

[12] F. Zhou, J. Li, H. Luo, F. Quellette, and Y. Liu, "Numerical analysis of 3.92 μm dual-wavelength pumped heavily-holmium-doped fluoroindate fiber lasers," *J. Lightw. Technol.*, vol. 39, no. 2, pp. 633–645, Jan. 2021.

[13] Z. Cheng et al., "Numerical modeling of dual-wavelength pumped heavily-Ho3+-doped fluoroindate fiber lasers with efficient output at 3.92 μm," *J. Lightw. Technol.*, vol. 41, no. 22, pp. 7021–7028, Nov. 2023.

[14] A. M. Loconsole, M. C. Falconi, A. Annunziato, S. Cozic, S. Poulain, and F. Prudenzano, "Design of a MID-IR laser based on a ho:Nd-codoped fluoroindate fiber," *J. Lightw. Technol.*, vol. 41, no. 2, pp. 702–708, Jan. 2023.

[15] Z. Zhang et al., "Enhanced 3.9 µm emission from diode pumped Ho3+/Eu3+ codoped fluoroindate glasses," *Opt. Lett.*, vol. 46, pp. 2031–2034, 2021.

[16] M. R. Majewski, R. I. Woodward, J.-Y. Carreé, S. Poulain, M. Poulain, and S. D. Jackson, "Emission beyond 4 μm and mid-infrared lasing in a dysprosium-doped indium fluoride (InF3) fiber," *Opt. Lett.*, vol. 43, pp. 1926–1929, 2018.

[17] Le Verre Fluoré, Catalog, 2022. [Online]. Available: https://leverrefluore.com/wp-content/uploads/2022/02/LVF-Catalog-2022.pdf

[18] M. R. Majewski and S. D. Jackson, "Numerical design of 4μm-class dysprosium fluoride fiber lasers," *J. Lightw. Technol.*, vol. 39, no. 15, pp. 5103–5110, Aug. 2021.

[19] R. S. Quimby and M. Saad, "Dy: Fluoroindate fiber laser at 4.5 μm with cascade lasing," in *Proc. Adv. Solid-State Lasers Congr.*, 2013, Paper AM 2A.7.

[20] G. Bolognesi et al., "Yellow laser performance of Dy3+ in co-doped Dy,Tb:LiLuF4," *Opt. Lett.*, vol. 39, no. 23, 2014, Art. no. 6628.

[21] H. He, Z. Jia, Y. Ohishi, W. Qin, and G. Qin, "Efficient 4 μm emission from Pr3+/Yb3+ co-doped fluoroindate glass," *Opt. Lett.*, vol. 46, pp. 5607–5610, 2021.

[22] D. Manzani, D. Pabœuf, S. J. L. Ribeiro, P. Goldner, and F. Bretenaker, "Orange emission in Pr3+-doped fluoroindate glasses," *Opt. Mater.*, vol. 35, no. 3, pp. 383–386, 2013.

[23] A. Remillieux et al., "Upconversion mechanisms of a praseodymium-doped fluoride fibre amplifier," *J. Phys. D: Appl. Phys.*, vol. 29, pp. 963–974, Jan. 1996.

[24] L. Gomes and S. D. Jackson, "Spectroscopic properties of ytterbium, praseodymium-codoped fluorozirconate glass for laser emission at 3.6 μm," *J. Opt. Soc. Amer. B*, vol. 30, pp. 1410–1419, 2013.

[25] R. Pappalardo, "Calculated quantum yields for photon-cascade emission (PCE) for Pr3+ and Tm3+ in fluoride hosts," *J. Lumin.*, vol. 14, pp. 159–163, 1976.

[26] R. S. Quimby and B. Zheng, "New excited state absorption measurement technique and application to Pr3+-doped fluorozirconate glass," *Appl. Phys. Lett.*, vol. 60, pp. 1055–1057, Mar. 1992.

Antonella Maria Loconsole received the M.Sc. degree in telecommunications engineering (*cum laude*) from Politecnico di Bari, Bari, Italy, in 2019, and the Ph.D. degree in electrical and information engineering in 2022. She is currently a Research Assistant in electromagnetic fields with the Department of Electrical and Information Engineering, Politecnico di Bari. Her research interests include optical fiber lasers and amplifiers, SIW antennas, and microwave applicators for medical applications.

Vito Vincenzo Francione received the M.Sc. degree in 2021 in automation engineering (*cum laude*) from Politecnico di Bari, Bari, Italy, where he is currently working toward the Ph.D. degree in electrical and information engineering. His research interests include optical fiber sensors, optical devices, antennas, and metamaterials.

Andrea Annunziato received the M.Sc. degree in electronic engineering (*cum laude*) in 2020 from Politecnico di Bari, Bari, Italy, where he is currently working toward the Ph.D. degree in aerospace sciences and engineering. His research interests include optical fiber sensors, lasers, and amplifiers.

Francesco Anelli (Student Member, IEEE) received the M.Sc. degree in 2021 in electronic engineering (*cum laude*) from Politecnico di Bari, Bari, Italy, where he is currently working toward the Ph.D. degree in electrical and information engineering. His research interests include the modeling and the characterization of antennas, metamaterials, optical fiber grating sensors, and optical devices for multi-spectral gas monitoring.

Francesco Prudenzano (Member, IEEE) received the Ph.D. degree in electronic engineering from Politecnico di Bari, Bari, Italy, in 1996. Since 2018, he has been a Full Professor of electromagnetic fields with the Department of Electrical and Information Engineering, Politecnico di Bari. He is currently the Head of Microwave and Optical Engineering Group, Department of Electrical and Information Engineering, Politecnico di Bari. He is involved in several national and international research projects and cooperations. He has coauthored more than 400 publications, 295 of which got published in journals and international conferences, lectures, and invited papers. His research interests include the design and characterization of microwave devices, integrated optics, and optical fiber-based devices. From 2017 to 2018, he was the Chair of SIOF, the Italian Society of Optics and Photonics (Italian branch of EOS—European Optical Society).

Open Access funding provided by 'Politecnico di Bari' within the CRUI CARE Agreement